


## Article

# Effect of Phosphorous Content on the Microstructure and Stress Rupture Properties of 15Cr–15Ni Titanium-Modified Austenitic Stainless Steel

Yufei Qiao<sup>1,2,3</sup>, Tian Liang<sup>1,3,\*</sup>, Sihan Chen<sup>1,2,3</sup>, Yuanyuan Ren<sup>4</sup>, Chunming Liu<sup>5</sup>, Yue Qi<sup>6</sup>, Yingche Ma<sup>1,3,\*</sup>  and Kui Liu<sup>1,3</sup>

- <sup>1</sup> CAS Key Laboratory of Nuclear Materials and Safety Assessment, Institute of Metal Research, Chinese Academy of Sciences, Shenyang 110016, China; yfqiao21b@imr.ac.cn (Y.Q.)
- <sup>2</sup> School of Materials Science and Engineering, University of Science and Technology of China, Hefei 230026, China
- <sup>3</sup> Shi-Changxu Innovation Center for Advanced Materials, Institute of Metal Research, Chinese Academy of Sciences, Shenyang 110016, China
- <sup>4</sup> China Institute of Atomic Energy, Beijing 102413, China
- <sup>5</sup> School of Materials Science and Engineering, Northeastern University, Shenyang 110819, China
- <sup>6</sup> Fushun Special Steel Shares Co., Ltd., Fushun 113006, China
- \* Correspondence: tliang@imr.ac.cn (T.L.); ycma@imr.ac.cn (Y.M.)

**Abstract:** The microstructure of solution-annealed and aged tensile properties and the stress rupture properties of 15Cr–15Ni titanium-modified austenitic stainless steel with different phosphorus contents were investigated using OM, SEM and TEM. The results showed that two phosphide morphologies were observed after long-term isothermal aging at 850 °C for 1000 h. One was the needle-like M<sub>2</sub>P distributed within the grain. The other was the blocky M<sub>3</sub>P distributed at the grain boundaries and twins. The tensile properties of the alloy were unaffected by the phosphorus content, but the stress rupture properties were significantly impacted. With the increase in the phosphorus content from 70 ppm to 250 ppm, the stress rupture life increased from 148 to 269.7 h. Since the strengthening effect of phosphides within the grain or at the grain boundary has been shown to improve the stress rupture properties of alloys, many nanosized granular precipitates, such as the sigma phase, carbides and phosphides, have been observed at the grain boundary, capable of alleviating the stress concentration and limit the crack propagation between two phases, improving the strength of the grain boundary. Intragranular needle-like phosphides can hinder dislocation movements effectively, which improves the intragranular strength of alloys.

**Keywords:** phosphorus; precipitation behavior; phosphides; stress rupture life; austenitic stainless steel



**Citation:** Qiao, Y.; Liang, T.; Chen, S.; Ren, Y.; Liu, C.; Qi, Y.; Ma, Y.; Liu, K. Effect of Phosphorous Content on the Microstructure and Stress Rupture Properties of 15Cr–15Ni Titanium-Modified Austenitic Stainless Steel. *Crystals* **2023**, *13*, 703. <https://doi.org/10.3390/cryst13040703>

Academic Editor: Sergio Brutti

Received: 16 March 2023

Revised: 9 April 2023

Accepted: 11 April 2023

Published: 20 April 2023



**Copyright:** © 2023 by the authors. Licensee MDPI, Basel, Switzerland. This article is an open access article distributed under the terms and conditions of the Creative Commons Attribution (CC BY) license (<https://creativecommons.org/licenses/by/4.0/>).

## 1. Introduction

15Cr–15Ni titanium-modified austenitic stainless steel (15–15Ti) is widely used for sodium-cooled fast reactor fuel cladding tubes, such as the AIM1 alloy in France, the D9 alloy in the United States and the Chs68 alloy in Russia [1]. This kind of material has good resistance to sodium-cooled corrosion, high-temperature mechanical properties and radiation resistance. It also has good weldability, as well as hot and cold processing performance [2–4]. However, with its radiation swelling resistance being weaker as compared to ferritic–martensitic steel and ODS steel, its applications in fast reactors have been limited [5]. Researchers [5–8] found that the addition of a small amount of alloying elements, such as Nb, P and Si, could improve the radiation swelling resistance of 15–15Ti austenitic stainless steel. The typical modified alloys include EK164 alloy, D9I alloy and 15-15SI. Compared to other alloying elements, phosphorous has been shown to be a more effective inhibitor of radiation swelling in austenitic stainless steel [8,9]. This is mainly because

needle-like phosphide precipitates act as recombination centers for trapping and absorbing point defects and gaseous helium atoms, which inhibit the nucleation of vacancies and interstitial atoms.

Phosphorus is an interesting element in stainless steel, having a long-standing reputation for causing temper embrittlement. Most previous experiments and electronic calculations [10,11] indicated that phosphorus segregated towards the grain boundary, leading to an embrittlement effect. White et al. [12] reported that phosphorus diffusion to vacancies decreased the surface energy and accelerated the cavity nucleation and growth in 304 austenitic stainless steels. Bandyopadhyay [13] found that phosphorus tended to segregate towards the grain boundaries, resulting in temper embrittlement in NiCrV steel. To prevent this embrittlement, Mo is often added to steel to improve its grain boundary cohesion. Therefore, phosphorus is traditionally deemed a harmful impurity in stainless steel, and excessive phosphorus would damage the mechanical properties of the alloy [13,14]. Y. Jin et al. [15] found that the increase in phosphorus content hindered the formation of fine MC carbides and favored the precipitation of coarse  $M_3C$  carbides in 1Cr-Mo-V steel, leading to the deterioration of creep properties. Similarly, Min-Ho Jang et al. [16] found that phosphorus promoted the precipitation of  $M_{23}C_6$ , while suppressing the precipitation of secondary NbC in the earlier stages of aging, accelerating the precipitation of the Laves phase. The Laves phase can deteriorate the creep properties in AFA austenite stainless steel. However, in Fe–Ni base alloys [17–19], phosphorus has been reported to have a positive effect on the stress rupture life without any obvious harmful effects on other mechanical properties, which was mainly attributed to the beneficial effect of phosphorus on grain boundaries. Y. Mandiang et al. [20] reported that phosphorus could improve the room temperature tensile properties of 316Ti austenitic stainless steel by promoting a large amount of fine carbides (MC carbides and  $M_{23}C_6$ ) or  $M_3P$  uniformly distributed in the matrix. Rowcliffe and Nicholson [21] found that phosphorus promoted the formation of needle-like phosphides, such as  $Cr_3P$ , nucleated on dislocation loops, resulting in an increase in the hardness of the Fe–18Cr–10Ni–0.3P alloy. Kegg et al. [22] indicated that a significant increase in the amount of fine intragranular  $M_{23}C_6$  could be achieved through the addition of phosphorus, increasing the hardness of austenitic stainless steel. As stated above, even though a lot of work has been conducted towards investigating the influence of phosphorus on the structure and mechanical properties of austenitic stainless steel, it still remains controversial, and its mechanism is not yet well understood. The traditional belief that phosphorus only affects the grain boundary has been challenged by the effect of phosphorus on intragranular precipitates. Therefore, it is crucial to comprehensively study the impact of phosphorus on both the grain boundary and intragranular region to understand its strengthening mechanism in austenitic stainless steel. Furthermore, there is limited research on the effect of phosphorus on the high-temperature stress rupture properties of austenitic stainless steel. Thus, it is necessary to investigate the influence of phosphorus on the instantaneous mechanical properties and high-temperature stress rupture properties of 15–15Ti austenitic stainless steel to gain a better understanding of its behavior.

In this work, various amounts of phosphorus were added to 15–15Ti austenitic stainless steel. An isothermal aging treatment and stress rupture experiments were carried out. The effect of phosphorus on the microstructure, instantaneous mechanical properties and the stress rupture properties of the 15–15Ti alloy were systematically studied. The aim of this study is to comprehensively investigate the influence of phosphorus on both the grain boundary and intragranular regions in order to better understand its strengthening mechanism in 15–15Ti austenitic stainless steel. This could provide valuable insights for alloy design and contribute to the improvement of the safe service life of cladding tubes.

## 2. Materials and Methods

Three different compositions of 15–15Ti austenitic stainless steel (15Cr–15Ni–Ti–xP alloy) were melted using vacuum induction melting (VIM) and cast into bars with a diameter of 100 mm and a weight of approximately 25 kg. The chemical compositions of these alloys are listed in Table 1 and were named 15Cr–15Ni–Ti–70P, 15Cr–15Ni–Ti–150P and 15Cr–15Ni–Ti–250P. The Thermo-calc2016b software (Thermo-calc Command System, TCFE8 thermodynamic database) was used to calculate the equilibrium phase mass fractions of each alloy as a function of temperature. The as-cast ingot was homogenized at 1200 °C for 12 h and then hot forged into a 50 × 50 mm square forging rod at an initial temperature of 1140 °C and a final temperature of 900 °C. The rods were then solution annealed at 1120 °C for 2 h, followed by water quenching to eliminate any thermally deformed structures. To expedite the precipitation of the secondary phases, an accelerated isothermal aging treatment was employed. The 15–15Ti–xP alloys were aged at 850 °C for 1000 h before being rapidly quenched in water.

**Table 1.** Measured chemical compositions of three kinds of alloys (wt.%).

Steel	C	Cr	Ni	Mo	Si	Mn	Ti	P	V	Fe
15Cr–15Ni–Ti–70P	0.056	16.03	15.20	2.20	0.44	1.51	0.40	0.007	0.20	Bal.
15Cr–15Ni–Ti–150P	0.058	15.99	15.18	2.17	0.41	1.55	0.40	0.018	0.19	Bal.
15Cr–15Ni–Ti–250P	0.059	15.99	15.11	2.17	0.45	1.54	0.40	0.026	0.19	Bal.

The metallographic specimens were prepared through grinding, mechanical polishing and then electrolytic etching with a chemical solution of 10% perchloric acid in an ethanol solution at room temperature and at 18 V. The amount, morphology, distribution and type of precipitates in the solution-treated and aged specimens were observed with optical microscopy (OM, Observer.Z1m) and a scanning electron microscope (SEM, Inspect S4800) equipped with an energy-dispersive spectrometer (EDS). Thin foils for TEM observations with thicknesses of at least 600 µm were cut from aging specimens and the gauge sections of the fractured specimens perpendicular to the loading axis. Then, the thin foils were mechanically thinned down to approximately 50 µm and electropolished in a chemical solution of 10 vol% perchloric acid and 90 vol% ethanol at 18–20 V and –20 to –25 °C. The crystal structural and chemical composition analyses of the precipitates were performed on a transmission electron microscope (TEM, FEI Talos) equipped with an energy-dispersive X-ray spectrometer (EDX).

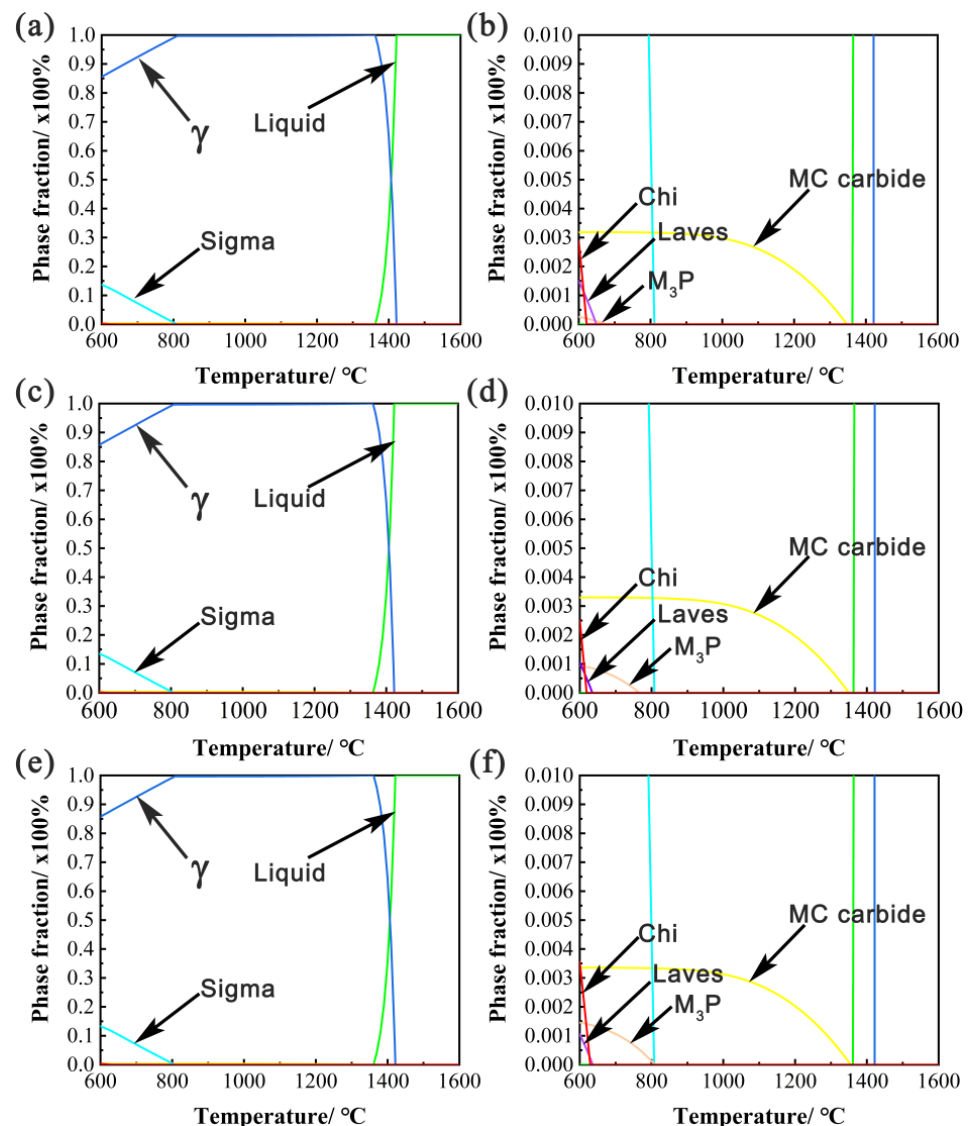
The standard M10 samples for the room temperature and 650 °C tensile tests were obtained through cutting from the long-term isothermal aging forging rods. The room temperature tensile tests were performed on the SANS-CMT 5205 tensile testing machine. The 650 °C tensile tests were performed on the INSTRON 5582 tensile testing machine. For the high-temperature stress rupture tests, standard M12 samples were prepared from the solution treatment forging rods and tested at 650 °C/195 MPa and 255 MPa. The stress rupture life and tensile properties were determined based on the average values. A scanning electron microscope (SEM, QUANTA 450) was used to observe the morphology and fracture behavior of the tensile and stress rupture fracture samples.

## 3. Results and Discussion

### 3.1. Effect of Phosphorus Content on Microstructure of 15Cr–15Ni Titanium-Modified Austenitic Stainless Steel during Long-Term Isothermal Aging

The equilibrium phase mass fractions of the 15Cr–15Ni–Ti–xP alloy were calculated using Thermo-calc2016b software over a temperature range of 600 to 1600 °C, as displayed in Figure 1. The liquidus temperature for the three alloys was approximately 1420 °C, as shown in the green line in the Figure 1, and the phase precipitated when the temperature was below 1420 °C. At temperatures below 1350 °C, the MC carbides precipitated with an amount of approximately 0.3 vol.%, as shown in the yellow line in the Figure 1. The sigma phases, M<sub>3</sub>P phosphide, Laves phase and Chi phase precipitated when the temperature

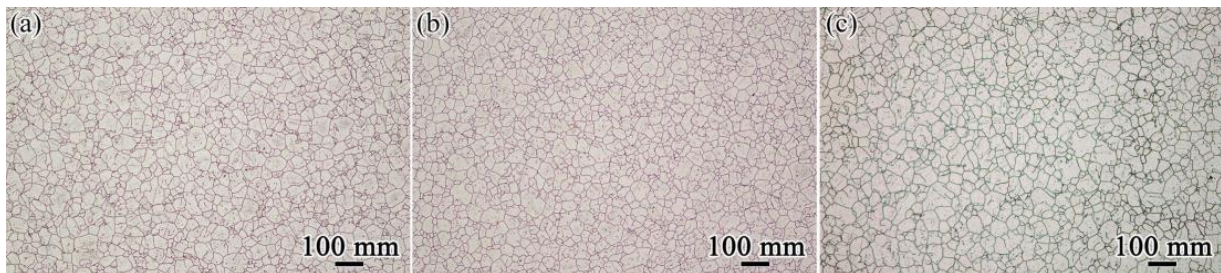
was below 805 °C, as shown in the light blue, dark yellow, purple and red lines in the Figure 1. The amounts of the sigma phase, Laves phase and Chi phase were found to be 14 vol.%, 0.15 vol.% and 0.3 vol.%, respectively. According to our results, the sigma phase, Laves phase and Chi phase were not significantly influenced by the phosphorus content. However, the precipitation temperatures of the  $M_3P$  phosphide increased from 680 to 805 °C, and the amount of precipitation increased from 0.1 to 0.15 vol.%, which indicates that elevated temperatures favored the precipitation of phosphides. Due to the sigma phase, Laves phase and Chi phase being essentially insensitive to changes in the phosphorus content, they did not deplete the P element. At the same time, the P diffusion capacity was strengthened in elevated temperatures. The phosphorus also preferred to aggregate at lattice defects (such as vacancies and dislocation defects), forming  $M_3P$  phosphides. Therefore, the amount of  $M_3P$  phosphides increased as the precipitation temperature rose.



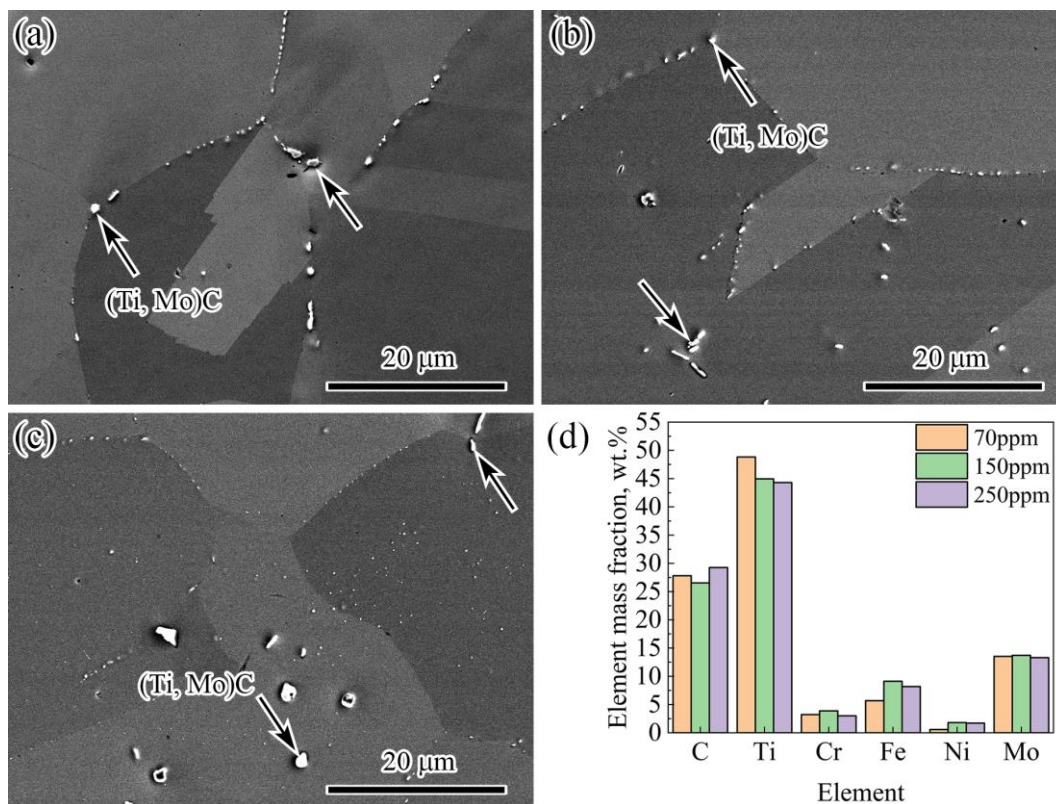
**Figure 1.** 15Cr–15Ni–Ti–xP alloy equilibrium phase fractions of precipitates calculated with ThermoCalc2016b. The whole and part of phase diagram about relationship between phases and temperature for (a,b) 15Cr–15Ni–Ti–70P alloy, (c,d) 15Cr–15Ni–Ti–150P alloy and (e,f) 15Cr–15Ni–Ti–250P alloy.

The microstructure of the 15Cr–15Ni–Ti–xP alloys after being solution treated at 1120 °C for 2 h is shown in Figure 2. The matrix structure of the 15Cr–15Ni–Ti–xP alloys with different phosphorous contents was shown to be an austenitic matrix with some precipitates after the solution treatment. The three alloys exhibited homogeneous and

fine equiaxed grains with an average grain size of approximately 23.87  $\mu\text{m}$ , 22.83  $\mu\text{m}$  and 28.75  $\mu\text{m}$ , separately. The average grain size of the three alloys was found to be similar, regardless of the phosphorus content, indicating that the phosphorus had no significant effect on the microstructure of the 15Cr–15Ni–Ti–xP alloys, as observed through the use of optical metallography. This was in accordance with previous research works [20,23]. In addition, a small amount of blocky MC carbides with grain sizes of approximately 1–2  $\mu\text{m}$  was detected in the matrix (shown by the black arrow in Figure 3). Moreover, some small and dispersed MC carbides were also found at the grain boundaries. According to the SEM-EDS analysis (Figure 3d), the MC carbides were rich in C, Ti and Mo, indicating that they were (Ti, Mo)C. Figure 3d shows a part of the SEM-EDS spectrum composition corresponding to the MC carbides, allowing for a comparison of the main components of the carbides.

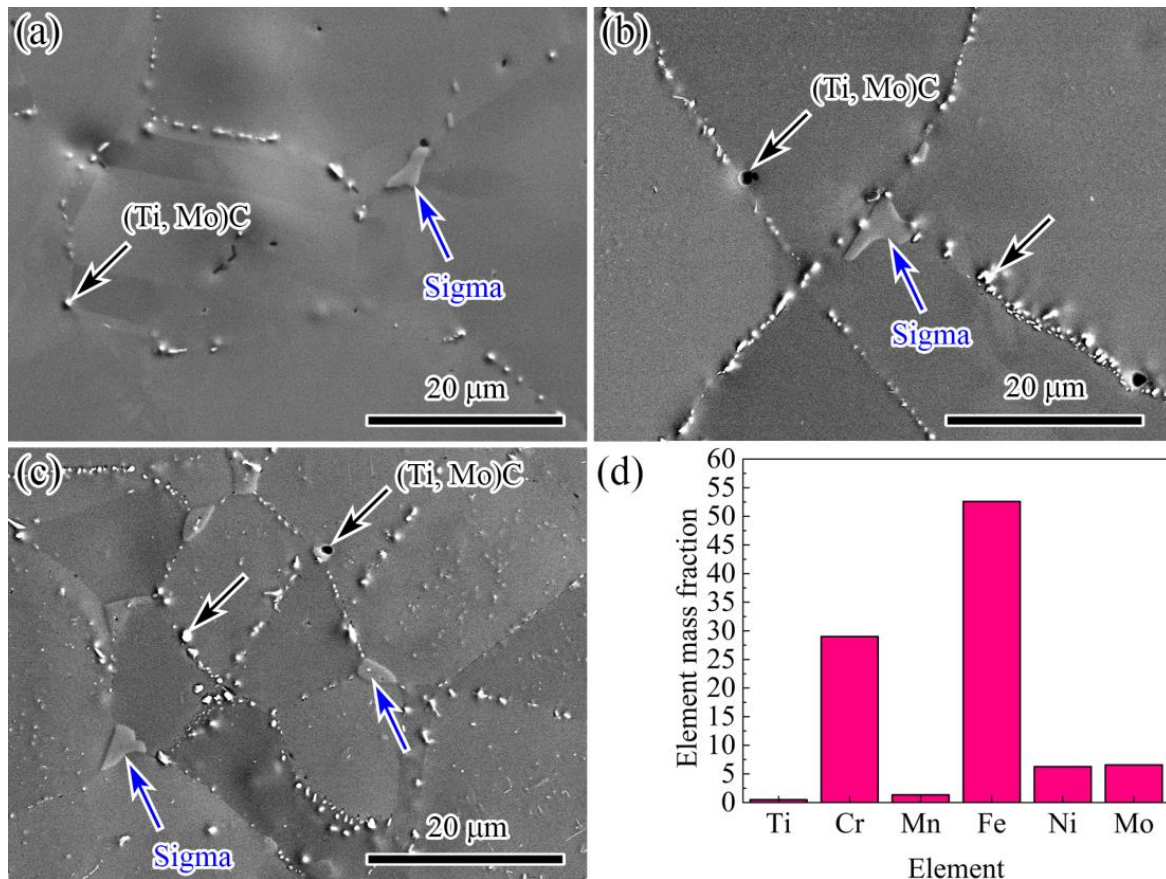


**Figure 2.** The optical microstructure of 15Cr–15Ni–Ti–xP alloy after being solution treated at 1120 °C for 2 h: (a) 15Cr–15Ni–Ti–70P alloy, (b) 15Cr–15Ni–Ti–150P alloy and (c) 15Cr–15Ni–Ti–250P alloy.



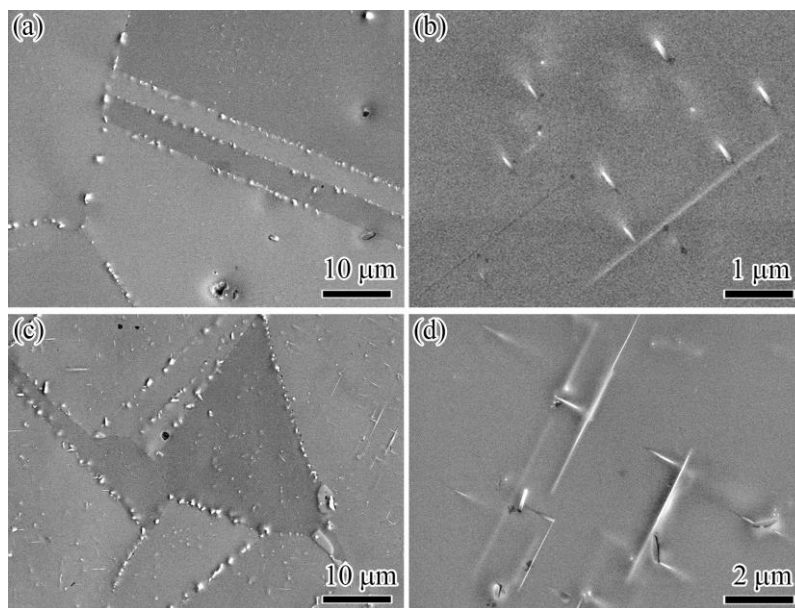
**Figure 3.** The SEM images of 15Cr–15Ni–Ti–xP alloy after being solution treated at 1120 °C for 2 h: (a) 15Cr–15Ni–Ti–70P alloy, (b) 15Cr–15Ni–Ti–150P alloy, (c) 15Cr–15Ni–Ti–250P alloy and (d) SEM-EDS spectrum corresponding to MC carbides.

Compared with the microstructure of the solution treatment, a large amount of phases precipitated in the 15Cr–15Ni–Ti–xP alloys after the aging treatment. In addition to some MC carbides (shown by the black arrow in Figure 4), a lot of new phases were also observed at the grain boundaries, with size ranges of approximately 3–8  $\mu\text{m}$  (shown by the blue arrow in Figure 4). According to the SEM-EDS analysis, the new phases were rich in Fe, Cr and Mo elements (Figure 4d), and were speculated to be the sigma phase.



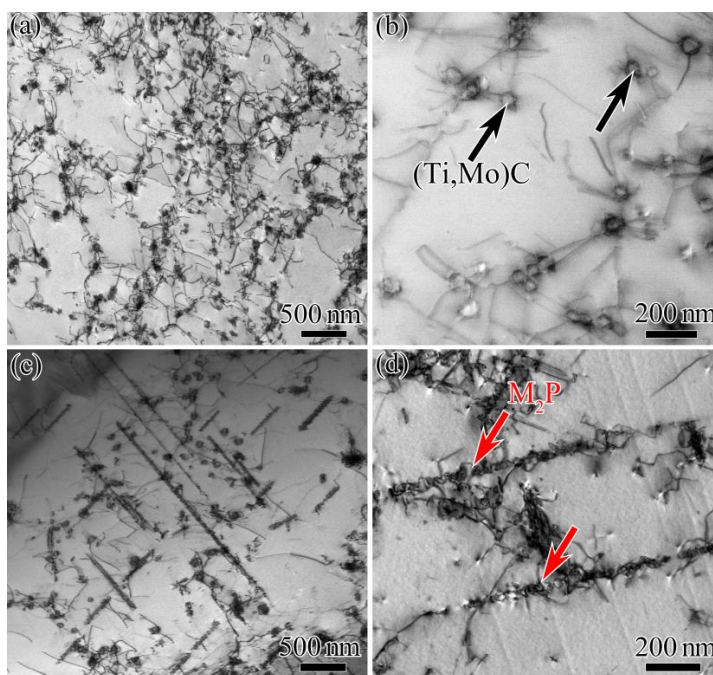
**Figure 4.** The SEM images of 15Cr–15Ni–Ti–xP alloys after aging at 850 °C for 1000 h: (a) 15Cr–15Ni–Ti–70P alloy, (b) 15Cr–15Ni–Ti–150P alloy, (c) 15Cr–15Ni–Ti–250P alloy and (d) SEM-EDS spectrum corresponding to sigma phase.

With the increase in the phosphorus content, it was observed that the number of these precipitates significantly increased. In addition to the sigma phase, phosphides were also found in the 15Cr–15Ni–Ti–150P and 15Cr–15Ni–Ti–250P alloys. Two phosphide morphologies were observed; one was a blocky phosphide distributed at the grain boundaries and twins, and the other was a needle-like phosphide distributed within the grain. In the 15Cr–15Ni–Ti–150P alloy, the needle-like precipitates with a size of approximately 0.5  $\mu\text{m}$  were primarily distributed within the twin boundaries and grains, as shown in Figure 5a,b. It is worth noting that in the 15Cr–15Ni–Ti–250P alloy, when the needle-like phases formed within the grain, their size was longer, ranging from approximately 2–5  $\mu\text{m}$ , as shown in Figure 5c,d.



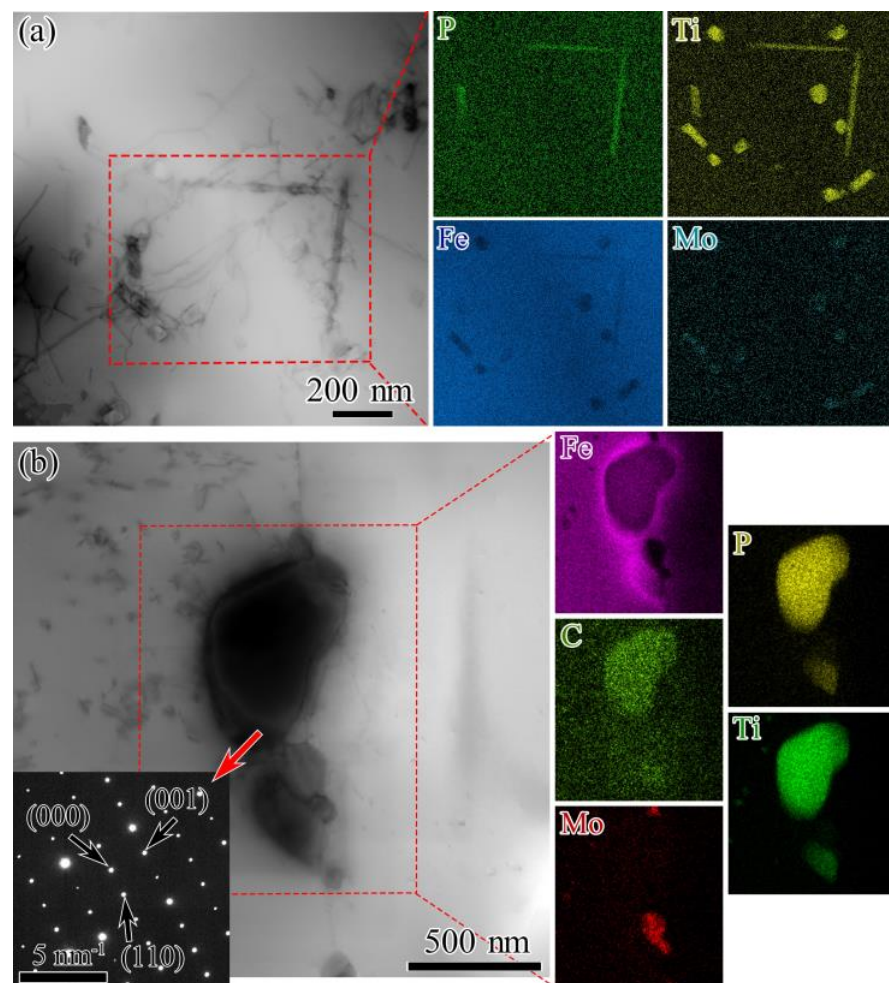
**Figure 5.** The SEM images of the 15Cr-15Ni-Ti-xP alloy after aging at 850 °C for 1000 h: (a,b) 15Cr-15Ni-Ti-150P alloy and (c,d) 15Cr-15Ni-Ti-250P alloy.

Figure 6 shows the TEM images of 15Cr-15Ni-Ti-xP alloy after aging at 850 °C for 1000 h. It can be seen that a large amount of nanosized carbides were observed within the grain, while needle-like phosphides were rarely observed, as shown in Figure 6a,b. However, as the phosphorus content increased to 250 ppm, a large number of needle-like phases and nanosized granular MC carbides were seen to precipitate within the grain, as shown in Figure 6c,d. This was attributed to the fact that phosphorus also has a tendency to aggregate at the dislocation within the grain after aging at 850 °C for 1000 h, which results in the precipitation of needle-like phosphides.



**Figure 6.** The TEM images of the 15Cr-15Ni-Ti-xP alloy after aging at 850 °C for 1000 h: (a,b) 15Cr-15Ni-Ti-150P alloy and (c,d) 15Cr-15Ni-Ti-250P alloy.

In recent years, the needle-like phosphides of type  $M_2P$  ( $Fe_2P$ ,  $NbNiP$  and  $FeTiP$ ) have been reported in phosphorous-containing austenitic stainless steels [7,24–26]. Bentley and Leitnaker [24,25] reported a kind of needle-like phase of type  $Fe_2P$ , with a lattice parameter of  $a = 0.608$  nm and  $c = 0.364$  nm, which grew in the (100) direction in type 321 stainless steel containing 0.03 wt.% P after 17 years of service aging at 600 °C. S. Latha [7] reported that under 973 K/150 MPa, the needle-like phosphides of type  $FeTiP$  were observed in 20% CW Ti-modified 14Cr–15Ni stainless steel. Chang-Wan Hong [26] found needle-like Nb-rich phosphides during a rupture test at 750 °C in a TP347H austenitic stainless steel, which were identified to be of the orthorhombic  $M_2P$  structure with the lattice parameters ( $a = 0.610$  nm,  $b = 0.357$  nm and  $c = 0.709$  nm) of  $NbNiP$ . In the present work, the needle-like phosphides were rich in Fe, Ti and P (shown in Figure 7a), which was consistent with the needle-like phase composition reported by S. Latha. Therefore, the needle-like phosphide in this study should have been of the type  $M_2P$  ( $FeTiP$ ).



**Figure 7.** The TEM images of the 15Cr–15Ni–Ti–250P alloy after aging at 850 °C for 1000 h: (a) needle-like phosphides and (b) blocky phosphides.

The blocky phosphide was also rich in Fe, Ti and P. The SAED patterns (shown in Figure 7b) indicated that the blocky phosphide had tetragonal system structures with the lattice parameters of  $a = b = 0.8936$  nm and  $c = 0.459$  nm, and should be classified as an  $M_3P$  phosphide. Compared with the needle-like  $M_2P$ , the blocky  $M_3P$  was also rich in C, which may have been because of some P atoms being replaced with C atoms. The previous literature [27] reported that some phosphorus atoms could be replaced with Si and S atoms during the formation of phosphides, indicating that the phosphides could accommodate a wide range of elements, including C. The morphology and composition of



the blocky phosphide also differed from the  $M_3P$  reported in previous studies. Rowcliffe and Nicholson [21] reported that after high-temperature aging, a large number of dispersed needle-like  $Cr_3P$  was found in the austenite matrix of the 18Cr–10Ni–0.3P alloy. Needle-like  $(Cr, Mo)_3P$  has also been reported in a Ti-modified 316 stainless steel containing 0.15 wt.% P during aging temperatures ranging from 600 to 800 °C [28]. In summary, when the 15Cr–15Ni–Ti–xP (x: 150–250 ppm) alloy was aged at 850 °C for 1000 h, two types of phosphides were precipitated; one was the needle-like  $M_2P$  that was rich in Fe, Ti and P, while the other was the blocky  $M_3P$ , which was rich in Fe, Ti, P and C.

### 3.2. Effect of Phosphorus Content on Tensile Properties of 15Cr–15Ni Titanium-Modified Austenitic Stainless Steel

Figure 8a shows the tensile properties of the 15Cr–15Ni–Ti–xP alloy at room temperature (RT) after aging at 850 °C for 1000 h. The phosphorus content increased from 70 ppm to 250 ppm, and the yield strength (YS), ultimate tensile strength (UTS) and elongation exhibited minimal changes. Figure 8b shows the tensile properties of the 15Cr–15Ni–Ti–xP alloy at 650 °C after aging at 850 °C for 1000 h, and it could be seen that the YS, UTS and elongation of the 15Cr–15Ni–Ti–xP alloy also showed slight variations. Therefore, it could be concluded that after aging at 850 °C for 1000 h, the phosphorus had little effect on the tensile properties of the 15Cr–15Ni–Ti–xP alloy at RT and 650 °C with a phosphorus content increasing from 70 to 250 ppm.

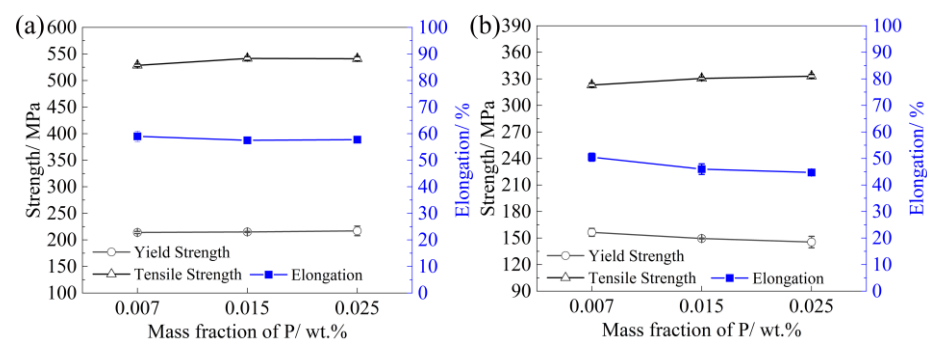


**Figure 8.** (a) Room temperature and (b) 650 °C tensile properties of 15Cr–15Ni–Ti–xP alloy after aging at 850 °C for 1000 h.

Figure 9 shows the SEM micrographs of the RT and 650 °C tensile fracture surfaces of the 15Cr–15Ni–Ti–xP alloy. A large number of dimples with varying depths was observed, distributed across the alloy's fracture surfaces at the RT. Moreover, numerous secondary cracks (as shown in the white circle in Figure 9a–c.) were observed on the fracture surfaces, with their number and size increasing as the phosphorus content increased. This indicated the ductile fracture to be of a typical mixed mode. Figure 9d–f show the tensile fracture surfaces of the 15Cr–15Ni–Ti–xP alloy at 650 °C. After tensile testing at 650 °C, necking was observed, and the fracture surfaces displayed a parabolic morphology with shallow dimples. The tensile fracture morphologies of the 15Cr–15Ni–Ti–xP alloy followed the ductile and transgranular fracture modes.

Previous research on austenitic stainless steel [20–22] showed that the addition of phosphorus resulted in the uniform distribution of a large amount of fine carbides (MC carbides and  $M_{23}C_6$ ) or  $M_3P$  in the matrix, which improved the alloy's mechanical properties. Other investigations on superalloys [19,23,29,30] were similar to ours. It is well known that the microstructure of an alloy is the key factor for determining its properties. Nevertheless, despite the presence of intragranular needle-like phosphides and blocky phosphides at the grain boundaries, which are expected to strengthen the alloy, the improvement in tensile properties was not observed in our research.

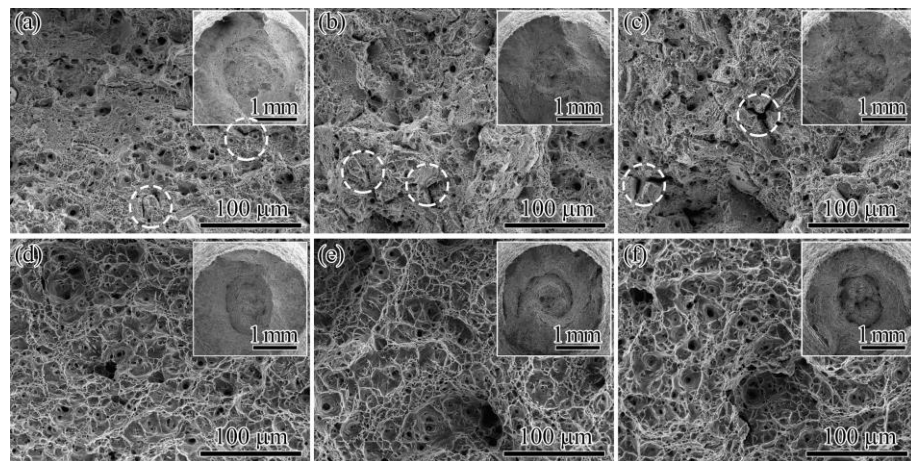


**Figure 9.** The SEM micrographs of (a–c) room temperature tensile fracture surfaces and (d–f) 650 °C tensile fracture surface after aging at 850 °C for 1000 h: (a,d) 15Cr–15Ni–Ti–70P alloy, (b,e) 15Cr–15Ni–Ti–150P alloy and (c,f) 15Cr–15Ni–Ti–250P alloy.

As shown in Figure 4a, little phosphides were observed in the 15Cr–15Ni–Ti–70P alloy, suggesting that phosphorus had a strengthening effect through the solution in the matrix. In the 15Cr–15Ni–Ti–150P alloy and 15Cr–15Ni–Ti–250P alloy, a large number of intragranular needle-like phosphides was observed after aging at 850 °C for 1000 h (Figures 4b,c and 5), but they did not seem to play a significant role in strengthening the alloy. Normally, P atoms tend to segregate at dislocation defects, which can pin and hinder the movement of the dislocations, thereby improving the tensile strength of alloys. However, in the tensile experiment, the high-stress and short-time loading process resulted in extremely fast dislocation movement speeds, which can eliminate the pinning effect of the P atoms [23]. This indicated that the phosphorus did not enhance the grain interior strength. After aging at 850 °C for 1000 h, a large number of blocky phosphides was also observed at the grain boundaries in the 15Cr–15Ni–Ti–150P and 15Cr–15Ni–Ti–250P alloys, suggesting that the phosphorus mainly strengthened the alloys through precipitation strengthening. Blocky phosphides at the grain boundaries could improve the grain boundary strength. However, the phosphorus did not fundamentally change the tensile fracture mode of the 15Cr–15Ni–Ti–xP alloys (Figure 9). The transgranular failure modes during the tensile process indicated that the tensile strength mainly depended on the grain interior strength rather than the grain boundary strength. Moreover, the phosphorus exhibited no obvious effect on the grain size of the 15Cr–15Ni–Ti–xP alloys (Figure 2). Therefore, we could conclude that the phosphorus had little effect on the tensile properties.

### 3.3. Effect of Phosphorus Content on the Stress Rupture Properties of 15Cr–15Ni Titanium-Modified Austenitic Stainless Steel

Figure 10a illustrates the stress rupture life of the 15Cr–15Ni–Ti–xP alloy at 650 °C/195 MPa after the solution treatment. The stress rupture life and ductility of the 15Cr–15Ni–Ti–70P alloy were 1302.5 h and 34.5%, respectively. The stress rupture life increased remarkably as the phosphorus content increased from 70 ppm to 150 ppm. When the phosphorus content increased to 250 ppm, the stress rupture life continued to increase to 1808 h, but the ductility reduced to 29.5%. It could be concluded that the stress rupture strength of the 15Cr–15Ni–Ti–xP alloys was highly dependent on the phosphorus content, and even slight changes in the phosphorus content could significantly affect the stress rupture strength. Figure 10b shows the stress rupture life of three alloys at 650 °C/255 MPa after the solution treatment. With the increase in the phosphorus content from 70 ppm to 150 ppm and 250 ppm, the stress rupture life increased from 148 h to 254.5 h and 269.7 h, respectively. However, the stress rupture ductility dropped slightly from 37.5% to 27% and 31%. The stress rupture life of the 15Cr–15Ni–Ti–250P alloy was almost twice that of the 15Cr–15Ni–Ti–70P alloy,

but the stress rupture ductility decreased only slightly. Therefore, it could be inferred that the addition of phosphorus optimized the stress rupture life of the 15Cr–15Ni–Ti–xP alloy. Since the stress rupture behavior under both stress conditions showed similar trends, the microstructure of the alloy at 650 °C/195 MPa was selected as a representative example for the analysis.

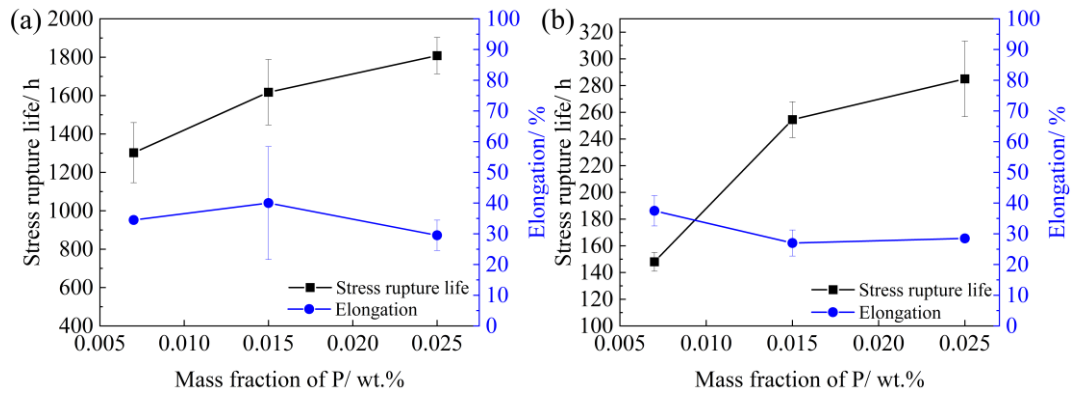


**Figure 10.** The stress rupture properties of 15Cr–15Ni–Ti–xP alloy after solution treated at 1120 °C for 2 h: (a) 650 °C/195 MPa; (b) 650 °C/255 MPa.

The stress rupture fracture morphology of the 15Cr–15Ni–Ti–xP alloys at 650 °C/195 MPa after the solution treatment was shown in Figure 11. A tearing edge with a smooth surface was observed at the edge of the specimens, as shown by the white circle in Figure 11a–c. The central area of the fracture was the plastic zone, and the morphology mainly comprised dimples of varying size, depth and shallowness, as shown in Figure 11d–f. The fracture modes of the three alloys exhibited a mixed mode of intergranular and ductile fracture, and their morphology did not show any significant changes with the varying phosphorus content.

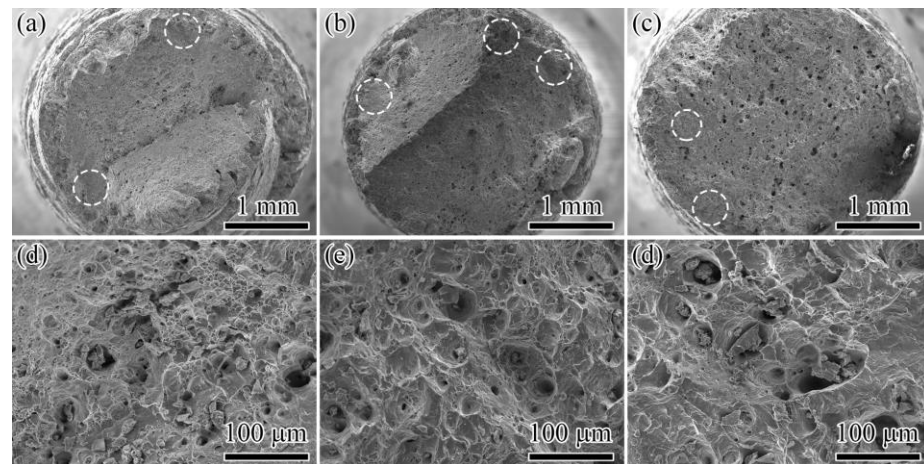


**Figure 11.** The stress rupture fracture surfaces of 15Cr–15Ni–Ti–xP alloy after stress rupture testing at 650 °C/195 MPa: (a,d) 15Cr–15Ni–Ti–70P, (b,e) 15Cr–15Ni–Ti–150P and (c,f) 15Cr–15Ni–Ti–250P.

To further investigate the reason behind the variations in the stress rupture life of the 15Cr–15Ni–Ti–xP alloys after the solution treatment, the longitudinal microstructure of the stress rupture specimens tested at 650 °C/195 MPa was observed, as shown in Figure 12. In the 15Cr–15Ni–Ti–70P alloys, cracks mainly originated from the large MC carbides that formed at the grain boundaries. A large number of pits near the phase was observed at the grain boundary, indicating that the cracks initiated and propagated at the interface between the phase and the matrix, leading to a reduction in the stress rupture life of the alloys. Conversely, in the 15Cr–15Ni–Ti–150P/250P alloys, the number of large MC

carbides reduced, while a significant number of fine sigma phases and phosphides were precipitated at the grain boundaries, as shown in the red box in Figure 12. However, the cracks around the small-sized phases were not observed.

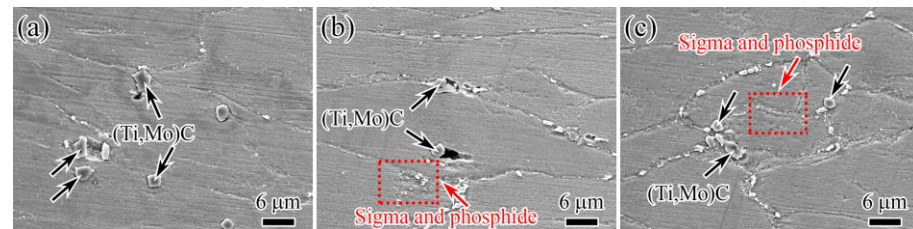


**Figure 12.** Microstructures of longitudinal section near tensile fracture surfaces of 15Cr–15Ni–Ti–xP alloy after stress rupture testing at 650 °C/195 MPa: (a) 15Cr–15Ni–Ti–70P alloy, (b) 15Cr–15Ni–Ti–150P alloy and (c) 15Cr–15Ni–Ti–250P alloy.

The effect of grain boundary precipitates on the creep or stress rupture life of the material was determined using various factors, such as the size, shape, amount and distribution at the grain boundaries [24,25,27,28,31–33]. Fine precipitates can inhibit the grain boundaries from sliding and prevent cracking. It is well known that adding Ti or Nb to stainless steel induces fine MC carbides, which interact with dislocations and hinder their movement, thereby enhancing the strength of the alloy [7,34]. Furthermore, adding phosphorous to the alloy also leads to the formation of fine phosphides, such as Nb-rich  $M_2P$ -type phosphides in TP347H austenitic stainless steel [26] and  $M_3P$ -type phosphides in 316Ti austenitic stainless steels [20]. In our work, in the 15Cr–15Ni–Ti–70P alloys, the sigma phase and MC carbides were found at the grain boundaries under the stress rupture condition of 650 °C/195 MPa, as shown in Figure 13a. Additionally, few phosphides were observed, which was consistent with the results of the long-term isothermal aging at 850 °C. I believe that P was present in the matrix mainly in the form of a solid solution due to the low content, which was reported in the IN706 alloy [35]. However, in the 15Cr–15Ni–Ti–250P alloys, a large number of nanosized phases, including the sigma phase,  $M_3P$  phosphide and MC carbide, was precipitated at the grain boundaries. This was attributed to the segregation of P atoms at the grain boundaries, which reduced the grain boundary energy and the critical nucleus radius of the precipitates [23,29,30]. As a result, a large number of nanosized sigma phases and phosphides was nucleated at the grain boundaries, as shown in Figure 13b. Compared to the 15Cr–15Ni–Ti–70P alloys, the number of nanosized sigma phases and phosphides significantly increasing at the grain boundaries in the 15Cr–15Ni–Ti–250P alloys, as shown in Figure 13b. The abundant nanosized granular precipitates at the grain boundary could alleviate the stress concentration in the matrix interface, which delayed the formation of cracks around the precipitates. At the same time, intergranular precipitates could effectively pin the grain boundaries and hinder grain sliding along the boundary, thereby strengthening the grain boundary. Moreover, the nanosized granular precipitates distributed along the grain boundary could limit crack propagation between two phases and make the cracks difficult to expand further, as shown in Figure 12. In the range of a reasonable phosphorus content, an increase in the amount of intergranular phosphides led to a more pronounced strengthening effect. Therefore, it can be concluded that the increase in the phosphorous content affected the morphology, quantity and distribution of the precipitates, which had a significant effect on the stress rupture properties of the 15Cr–15Ni–Ti–xP alloys.

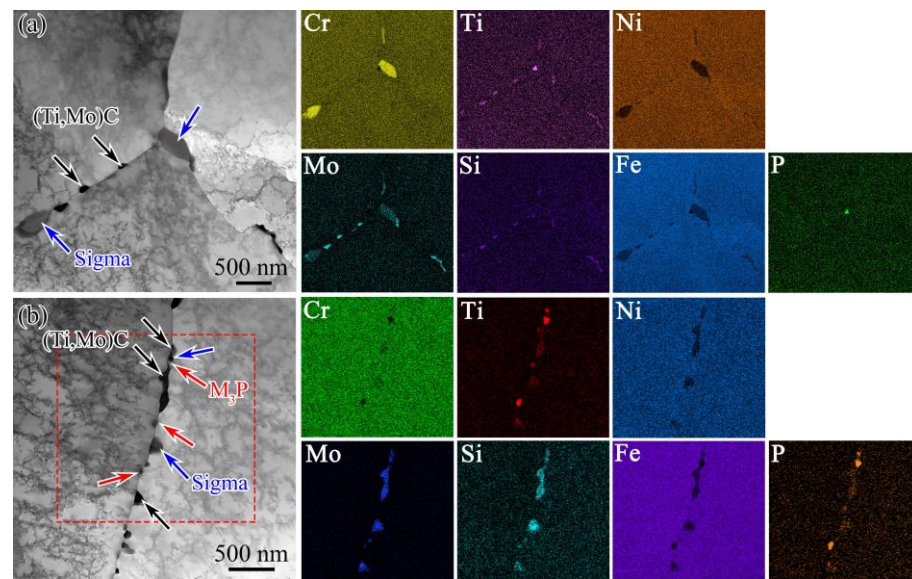


**Figure 13.** The TEM images near fracture surface of 15Cr–15Ni–Ti–xP alloy after stress rupture testing at 650 °C/195 MPa: (a) 15Cr–15Ni–Ti–70P alloy and (b) 15Cr–15Ni–Ti–250P alloy.

The quantity and size of the blocky MC carbides reduced with the increase in the phosphorous content, since P consumed Ti atoms and formed phosphides. It could be seen from the results of the equilibrium phase calculation (Figure 1) that the precipitation temperatures of the  $M_3P$  phosphide was enhanced from 680 to 805 °C with the rise in the phosphorus content, which was beneficial for promoting the precipitation of phosphides. Nam et al. [36] believed that the density of the carbides at the grain boundary decreased in AISI304L stainless steel with the increase in the phosphorus content, which indicated the beneficial effect of phosphorus on the fatigue life under creep–fatigue testing at 823K. Moreover, microvoids formed easily at the interface between the matrix and MC carbides, which propagated and connected with each other, ultimately leading to intergranular cracks [37]. Thus, the decrease in MC carbides due to the phosphorous (shown in Figure 12) was beneficial for the stress rupture life of the 15Cr–15Ni–Ti–xP alloys.

Previous research work has shown that phosphorus affects the grain boundary of austenitic stainless steel due to its serious trend of segregation along the grain boundary [38–40]. Nevertheless, it has been recently found that the intragranular structure can also be affected by adding phosphorus [35,41,42]. Therefore, it is essential to investigate whether phosphorus also has a strengthening effect on the intragranular region.

It is well known that phosphorus also prefers to aggregate at lattice defects (such as vacancies and dislocation defects), forming intragranular precipitates [27,28,31]. In our work, after being aged at 850 °C for 1000 h, the quantity of needle-like phosphides within the grain increased significantly with the increase in the phosphorus content (Figures 4 and 5). This indicated that phosphorus did not only have an effect on the grain boundary, but also affected the intragranular region. Due to the applied stress during the stress rupture tests being smaller than that during the tensile test, dislocations had difficulty in removing the pinning effect of the intragranular phosphides. As shown in Figure 6, intragranular needle-like phosphides could effectively hinder dislocation movements, negatively affecting the plastic deformation of the alloy. This explains why the increase in the phosphorous content causes the stress rupture elongation to decrease in the alloys. The intragranular strength is closely related to the number of precipitated strengthening phases [43,44]. The more intragranular needle-like phosphides, the more difficult are the dislocations moving to the grain boundary, and the less stress concentrates around the grain boundary [45]. A much larger amount of applied stress was needed to induce adjoining grains to deform plastically, which meant that the intragranular strength increased with the increase in the phosphorus content. To sum up, the new finding of phosphide’s strengthening effect within the grain

or at the grain boundary could provide a critical reference point for further understanding the effect of phosphorous on the mechanical properties of austenitic stainless steel.

#### 4. Conclusions

In the present study, the effect of phosphorous addition on the precipitation behavior and stress rupture properties was investigated in 15Cr–15Ni–Ti–xP (x: 0–250 ppm) alloys. From the microstructure analyses combined with the stress rupture properties, the following specific conclusions could be drawn:

According to the thermodynamic equilibrium phase diagram, the amount of phosphides increased as the precipitation temperature rose. This was mainly due to the fact that the P element could not be depleted through the sigma phase, Laves phase or Chi phase, and the P diffusion capacity was strengthened with elevated temperatures.

After aging at 850 °C for 1000 h, two phosphide morphologies were precipitated in the 15Cr–15Ni–Ti–xP alloys with the phosphorous content ranging from 150 ppm to 250 ppm. One was the needle-like  $M_2P$  distributed within the grains and enriched in Fe, Ti and P. The other was the blocky  $M_3P$  distributed at the grain boundaries and twins and enriched in Fe, Ti, P and C.

The tensile properties of the alloy were unaffected by the phosphorus content, which was attributed to the fact that tensile strength mainly depends on the grain interior strength rather than the grain boundary strength.

The stress rupture properties were significantly impacted by the phosphorus content. This was mainly because many nanosized granular precipitates, such as the sigma phase, carbides and phosphides, were observed at the grain boundary, which could alleviate the stress concentration and limit the crack propagation between two phases, improving the strength of the grain boundary. Intragranular needle-like phosphides could effectively hinder dislocation movements, which improved the intragranular strength of the alloy.

**Author Contributions:** Conceptualization, methodology, data curation and writing—original draft: Y.Q. (Yufei Qiao); project administration, funding acquisition and writing—review and editing: T.L.; validation and methodology: S.C.; methodology and writing—review and editing: Y.R.; supervision: C.L.; writing—review and editing: Y.Q. (Yue Qi); supervision: Y.M.; supervision: K.L. All authors have read and agreed to the published version of the manuscript.

**Funding:** This research received no external funding.

**Data Availability Statement:** Data will be made available on request.

**Conflicts of Interest:** The authors declare no conflict of interest.

#### References

1. Buckthorpe, D. Introduction to Generation IV nuclear reactors. In *Structural Materials for Generation IV Nuclear Reactors*; Yvon, P., Ed.; Elsevier Ltd.: Amsterdam, The Netherlands, 2017; pp. 1–22.
2. Murty, K.L.; Charit, I. Structural materials for Gen-IV nuclear reactors: Challenges and opportunities. *J. Nucl. Mater.* **2008**, *383*, 189–195. [[CrossRef](#)]
3. Hari Krishan Yadav, A.R.; Ballal, M.M. Creep studies of Cold Worked Austenitic Stainless Steel. *Procedia Struct. Integr.* **2019**, *14*, 605–611. [[CrossRef](#)]
4. Wang, Z.N.; Liang, T.; Xing, W.W.; Du, A.B.; Gao, M.; Ma, Y.C.; Liu, K.  $\sigma$ -Phase Precipitation Mechanism of 15Cr–15Ni Titanium Modified Austenitic Stainless Steel During Long-Term Thermal Exposure. *Acta Metall. Sin.* **2018**, *31*, 281–289. [[CrossRef](#)]
5. Jayakumar, T.; Mathew, M.D.; Laha, K.; Sandhya, R. Materials development for fast reactor Applications. *Nucl. Eng. Des.* **2013**, *265*, 1175–1180. [[CrossRef](#)]
6. Séran, J.L.; Le Flem, M. Irradiation-resistant austenitic steels as core materials for Generation IV nuclear reactors. In *Structural Materials for Generation IV Nuclear Reactors*; Yvon, P., Ed.; Woodhead Publishing: Sawston, UK, 2017; pp. 285–328.
7. Latha, S.; Mathew, M.D.; Parameswaran, P.; Nandagopal, M.; Mannan, S.L. Effect of titanium on the creep deformation behavior of 14Cr–15Ni–Ti stainless steel. *J. Nucl. Mater.* **2011**, *409*, 214–220. [[CrossRef](#)]
8. Chen, S.H.; Xie, A.; Lv, X.L.; Chen, S.H.; Yan, C.G.; Jiang, H.C.; Rong, L.J. Tailoring Microstructure of Austenitic Stainless Steel with Improved Performance for Generation-IV Fast Reactor Application: A Review. *Crystals* **2023**, *13*, 268. [[CrossRef](#)]

9. Mathew, M.D.; Gopal, K.A.; Murugan, S.; Panigrahi, B.K.; Bhaduri, A.K.; Jayakumar, T. Development of IFAC-1 SS: An Advanced Austenitic Stainless Steel for Cladding and Wrapper Tube Applications in Sodium Cooled Fast Reactors. *Adv. Mater. Res.* **2013**, *794*, 749–756. [[CrossRef](#)]
10. Wang, C.Y. Electronic Structure of Impurity-Defect Complexes in Metals. *Defect Diffus. Forum* **1995**, *125–126*, 79. [[CrossRef](#)]
11. Rice, J.R.; Wang, J.S. Embrittlement of interfaces by solute segregation. *Mater. Sci. Eng. A* **1989**, *107*, 23–40. [[CrossRef](#)]
12. White, C.L.; Padgett, R.A.; Swindeman, R.W. Sulfur and phosphorus segregation to creep cavities and grain boundaries in 304 SS. *Scr. Metall.* **1981**, *15*, 777–782. [[CrossRef](#)]
13. Bandyopadhyay, N.; Briant, C.L.; Hall, E.L. Carbide precipitation, grain boundary segregation, and temper embrittlement in NiCrMoV rotor steels. *Metall. Trans. A* **1985**, *16*, 721–737. [[CrossRef](#)]
14. Briant, C.L. Grain boundary segregation of phosphorus in 304L stainless steel. *Metall. Trans. A* **1985**, *16*, 2061–2062. [[CrossRef](#)]
15. Yu, J.; Grabke, H.J. Effects of P addition on creep of 1 Cr–Mo–V steels. *Met. Sci. J.* **1983**, *17*, 389–396. [[CrossRef](#)]
16. Jang, M.H.; Kang, J.Y.; Jang, J.H.; Lee, T.H.; Lee, C. The role of phosphorus in precipitation behavior and its effect on the creep properties of alumina-forming austenitic heat-resistant steels. *Mater. Sci. Eng. A* **2016**, *684*, 14–21. [[CrossRef](#)]
17. Yang, S.L.; Sun, W.R.; Wang, J.X.; Ge, Z.M.; Guo, S.R.; Hu, Z.Q. Effect of Phosphorus on Mechanical Properties and Thermal Stability of Fine-grained GH761 Alloy. *J. Mater. Sci. Technol.* **2011**, *27*, 539–545. [[CrossRef](#)]
18. Bika, D.; McMahon, C.J. A model for dynamic embrittlement. *Acta Metall. Mater.* **1995**, *43*, 1909–1916. [[CrossRef](#)]
19. Xue, C.C.; Liu, F.; Yao, X.Y.; Liu, D.Y.; Xin, X.; Sun, W.R.; Zhang, A.W.; Zhang, S. The existence and strengthening mechanism of phosphorus in Ni17Cr15Fe-based alloys. *Mater. Sci. Eng. A* **2020**, *797*, 140044. [[CrossRef](#)]
20. Mandiang, Y.; Ciss, A.; Sissoko, G.; Cizeron, G. Influence of thermal aging on microstructural evolution and mechanical properties in titanium modified type 316 stainless steel containing phosphorus. *Met. Sci. J.* **2001**, *17*, 315–320. [[CrossRef](#)]
21. Rowcliffe, A.F.; Nicholson, R.B. Quenching defects and precipitation in a phosphorus-containing austenitic stainless steel. *Acta Metall.* **1972**, *20*, 143–155. [[CrossRef](#)]
22. Kegg, G.R.; Silcock, J.M.; West, D.R.F. The Effect of Phosphorus Additions and Cooling Rate on the Precipitation of M23C6 in Austenite. *Met. Sci. J.* **1973**, *8*, 337–343. [[CrossRef](#)]
23. Guan, S.; Cui, C.Y.; Yuan, Y.; Gu, Y.F. The role of phosphorus in a newly developed Ni-Fe-Cr-based wrought superalloy. *Mater. Sci. Eng. A* **2016**, *662*, 275–282. [[CrossRef](#)]
24. Bentley, J.; Leitnaker, J.M. *Stable Phases in Aged Type 321 Stainless Steel*; Collings, E.W., King, H.W., Eds.; The Metal Science of Stainless Steels; TMS AIME: Warrendale, PA, USA, 1979; pp. 70–71.
25. Leitnaker, J.M.; Bentley, J. Precipitate phases in type 321 stainless steel after aging 17 years at ~600 °C. *Metall. Trans. A* **1977**, *8*, 1605–1613. [[CrossRef](#)]
26. Hong, C.W.; Heo, Y.U.; Heo, N.H.; Kim, S.J. Precipitation correlation between MC carbide and Nb-rich M<sub>2</sub>P phosphide in a TP347H austenitic stainless steel. *Mater. Charact.* **2016**, *124*, 192–205. [[CrossRef](#)]
27. Lee, E.H.; Mansur, L.K. Fe–15Ni–13Cr austenitic stainless steels for fission and fusion reactor applications. III. Phase stability during heavy ion irradiation. *J. Nucl. Mater.* **2000**, *287*, 20–29. [[CrossRef](#)]
28. Mandiang, Y.; Cizeron, G. Precipitation of M<sub>3</sub>P phosphide in titanium modified type 316 stainless steel. *Mater. Sci. Technol.* **2014**, *9*, 771–775. [[CrossRef](#)]
29. Yang, S.L.; Sun, W.R.; Wang, J.X.; Wang, K.L.; Guo, S.R.; Hu, Z.Q. Effect of P content on mechanical properties of fine-grained GH761 alloy. *Acta Metall. Sin.* **2009**, *45*, 815–819.
30. Xiao, X.; Zhao, H.Q.; Wang, C.S.; Guo, Y.A.; Guo, J.T.; Zhou, L.Z. Effect of B and P on microstructure and mechanical properties of GH984 alloy. *Acta Metall. Sin.* **2013**, *49*, 421–427. [[CrossRef](#)]
31. Lee, E.H.; Mansur, L.K. Fe-15Ni-13Cr austenitic stainless steels for fission and fusion reactor applications. II. Effects of minor elements on precipitate phase stability during thermal aging. *J. Nucl. Mater.* **2000**, *278*, 11–19. [[CrossRef](#)]
32. Lee, K.H.; Park, D.B.; Kwun, S.I.; Huh, J.Y.; Suh, J.Y.; Shim, J.H.; Jung, W.S. Effect of Creep deformation on the microstructural evolution of 11CrMoVNb heat resistant steel. *Mater. Sci. Eng. A* **2012**, *536*, 92–97. [[CrossRef](#)]
33. Laha, K.; Kyono, J.; Shinya, N. Suppression of creep cavitation in precipitation-hardened austenitic stainless steel to enhance creep rupture strength. *Trans. Ind. Inst. Met.* **2010**, *63*, 437–441. [[CrossRef](#)]
34. Fujiwara, M.; Uchida, H.; Ohta, S. Effect of niobium content on creep strength of coldworked 15Cr-15Ni-2.5Mo austenitic steel. *J. Mater. Sci. Lett.* **1995**, *14*, 297–301. [[CrossRef](#)]
35. Zhang, S.; Xin, X.; Yu, L.X.; Zhang, A.W.; Sun, W.R.; Sun, X.F. Effect of phosphorus on the grain boundary cohesion and  $\gamma'$  precipitation in IN706 alloy. *Metall. Mater. Trans.* **2016**, *47*, 4092–4103. [[CrossRef](#)]
36. Yoon, Y.C.; Kim, J.J.; Wee, D.M.; Nam, S.W. Effect of Phosphorus on the Creep–Fatigue Interaction in AISI 304 L Stainless Steel. *J. Korean Inst. Met. Mater.* **1992**, *30*, 1401–1406.
37. Wang, T.T.; Wang, C.S.; Sun, W.; Qin, X.Z.; Guo, J.T.; Zhou, L.Z. Microstructure evolution and mechanical properties of GH984G alloy with different Ti/Al ratios during long-term thermal exposure. *Mater. Des.* **2014**, *62*, 225–232. [[CrossRef](#)]
38. Wang, M.Q.; Du, J.H.; Deng, Q.; Tian, Z.L.; Zhu, J. The effect of phosphorus on the microstructure and mechanical properties of ATI 718Plus alloy. *Mater. Sci. Eng. A* **2015**, *626*, 382–389. [[CrossRef](#)]
39. Wang, M.Q.; Du, J.H.; Deng, Q.; Tian, Z.L.; Zhu, J. Effect of the precipitation of the  $\eta$ -Ni<sub>3</sub>Al<sub>0.5</sub>Nb<sub>0.5</sub> phase on the microstructure and mechanical properties of ATI 718Plus. *J. Alloys Compd.* **2017**, *701*, 635–644. [[CrossRef](#)]

40. Ping, D.H.; Gu, Y.F.; Cui, C.Y.; Harada, H. Grain boundary segregation in a Ni–Fe-based (Alloy 718) superalloy. *Mater. Sci. Eng. A* **2007**, *456*, 99–102. [[CrossRef](#)]
41. Zhang, A.W.; Zhang, S.; Liu, F.; Qi, F.; Yao, X.Y.; Tan, Y.G.; Jia, D.; Sun, W.R. Effect of cooling rate on phosphorus segregation behavior and the corresponding precipitation of  $\gamma''$  and  $\gamma'$  phases in IN718 alloy. *J. Mater. Sci. Technol.* **2019**, *35*, 1485–1490. [[CrossRef](#)]
42. Zhang, A.W.; Yang, Y.; Zhang, S.; Zhang, D.; Zhang, W.H.; Han, D.W.; Qi, F.; Tan, Y.G.; Xin, X.; Sun, W.R. Distribution of phosphorus and its effects on precipitation behaviors and tensile properties of IN718C cast superalloy. *Acta Metall. Sin.* **2019**, *32*, 887–899. [[CrossRef](#)]
43. Wu, R.H.; Yue, Z.F.; Wang, F.M. Effect of initial  $\gamma/\gamma'$  microstructure on creep of single crystal nickel-based superalloys: A phase-field simulation incorporating dislocation dynamics. *J. Alloys Compd.* **2019**, *779*, 326–334. [[CrossRef](#)]
44. Li, H.; Song, H.; Liu, W.L. The coarsening behavior of  $\gamma'$ -Ni<sub>3</sub>(Ti, Al) phase in a precipitation strengthened Fe-based alloy. *Mater. Char.* **2019**, *151*, 390–395. [[CrossRef](#)]
45. Cui, Y.N.; Po, G.; Ghoniem, N.M. A coupled dislocation dynamics-continuum barrier field model with application to irradiated materials. *Int. J. Plast.* **2018**, *104*, 54–67. [[CrossRef](#)]

**Disclaimer/Publisher’s Note:** The statements, opinions and data contained in all publications are solely those of the individual author(s) and contributor(s) and not of MDPI and/or the editor(s). MDPI and/or the editor(s) disclaim responsibility for any injury to people or property resulting from any ideas, methods, instructions or products referred to in the content.